Local electric dipole moments for periodic systems via density functional theory embedding

Luber, Sandra

Abstract: We describe a novel approach for the calculation of local electric dipole moments for periodic systems. Since the position operator is ill-defined in periodic systems, maximally localized Wannier functions based on the Berry-phase approach are usually employed for the evaluation of local contributions to the total electric dipole moment of the system. We propose an alternative approach: within a subsystem-density functional theory based embedding scheme, subset electric dipole moments are derived without any additional localization procedure, both for hybrid and non-hybrid exchange–correlation functionals. This opens the way to a computationally efficient evaluation of local electric dipole moments in (molecular) periodic systems as well as their rigorous splitting into atomic electric dipole moments. As examples, Infrared spectra of liquid ethylene carbonate and dimethyl carbonate are presented, which are commonly employed as solvents in Lithium ion batteries.

DOI: https://doi.org/10.1063/1.4903828

AIP | The Journal of Chemical Physics

Local electric dipole moments for periodic systems via density functional theory embedding

Sandra Luber

Citation: The Journal of Chemical Physics **141**, 234110 (2014); doi: 10.1063/1.4903828
View online: http://dx.doi.org/10.1063/1.4903828
View Table of Contents: http://scitation.aip.org/content/aip/journal/jcp/141/23?ver=pdfcov
Published by the AIP Publishing

Local electric dipole moments for periodic systems via density functional theory embedding

Sandra Luber[a)]
Institut für Chemie, Universität Zürich, Winterthurerstrasse 190, 8057 Zürich, Switzerland

(Received 23 September 2014; accepted 28 November 2014; published online 17 December 2014)

We describe a novel approach for the calculation of local electric dipole moments for periodic systems. Since the position operator is ill-defined in periodic systems, maximally localized Wannier functions based on the Berry-phase approach are usually employed for the evaluation of local contributions to the total electric dipole moment of the system. We propose an alternative approach: within a subsystem-density functional theory based embedding scheme, subset electric dipole moments are derived without any additional localization procedure, both for hybrid and non-hybrid exchange–correlation functionals. This opens the way to a computationally efficient evaluation of local electric dipole moments in (molecular) periodic systems as well as their rigorous splitting into atomic electric dipole moments. As examples, Infrared spectra of liquid ethylene carbonate and dimethyl carbonate are presented, which are commonly employed as solvents in Lithium ion batteries. © *2014 AIP Publishing LLC*. [http://dx.doi.org/10.1063/1.4903828]

I. INTRODUCTION

Knowledge about electric dipole moments is important for the analysis of a variety of materials ranging from molecules in gas phase up to condensed matter. Infrared (IR) spectroscopy, which probes changes in electric dipole moments, is nowadays routinely applied in chemical laboratories. For a detailed interpretation of experimental IR spectra, calculations are an indispensable tool leading to a deeper understanding of the structure and dynamics of the system under investigation. Simulation of IR spectra can be achieved by computing the electric dipole moment time autocorrelation function obtained from density functional theory (DFT)-based molecular dynamics (MD).[1,2] In contrast to static calculations,[3–13] this approach naturally takes into account the dynamics of the studied system at ambient conditions. In order to be able to discriminate the contributions of different components in the system, it is necessary to evaluate not only the total electric dipole moment of the system but also local electric dipole moments. The latter can be employed for the computation of IR spectra for the subsystem of interest.

In simulations for periodic systems such as liquids and solids, care has to be taken since the position operator, needed for the calculation of the electric dipole, is ill-defined. In this case, the Berry-phase formulation for the electric polarization[14–16] can be employed (for details about implementations regarding IR intensities for periodic systems, we refer to Refs. 17–20 and references cited therein). Local electric dipole moments can be computed by localization of Wannier functions.[21–30]

In this paper, an alternative approach to the evaluation of local electric dipole moments is presented. We rely on subsystem DFT-based embedding (for the sake of brevity, in the following partly only referred to as "embedding") where the total electronic density is divided into electronic densities of subsystems.[31–36] The interaction between the subunits is included by local external embedding potentials. Moreover, it is an appealing approach for the treatment of large systems at reduced computational cost. Subsystem electronic densities can be obtained via a more accurate (and computationally more expensive) method whereas the interactions between the subsystems can be calculated by a less sophisticated method with lower computational effort. In most present-day applications, Kohn–Sham (KS)-DFT[37] has been employed as the more accurate method whereas the orbital-free Hohenberg–Kohn (HK) formulation[38] has been used for treating the interactions between the subsystems. This subsystem formulation is in principle exact in case of exact density functionals, given that the subsystem electronic densities are v_s representable,[39–41] and is currently mainly limited due to the approximations in kinetic energy (KE) functionals. It has been applied in numerous applications to the modelling both of ground state[35,42–61] and excited-state related properties.[62–77] Instead of KS-DFT, other electronic-structure methods have also been employed.[62,64,78–83]

We use a computationally efficient embedding approach, which takes periodic boundary conditions into account[52,84] and treats all subsystems on equal footing. This allows us to derive local electric dipole moments for periodic systems without resorting to additional localization procedures as is necessary, e.g., in the case of the commonly employed maximally localized Wannier functions (MLWFs). Moreover, our formulation can be applied in density matrix-based linear scaling DFT calculations as, e.g., implemented in the CP2K program package.[85] Fragmentation techniques such as the fragment molecular orbital[86] or absolutely localized molecular orbital method[87] may be a valuable alternative, which, to the best of our knowledge, have not been applied to the

a)Email: sandra.luber@chem.uzh.ch

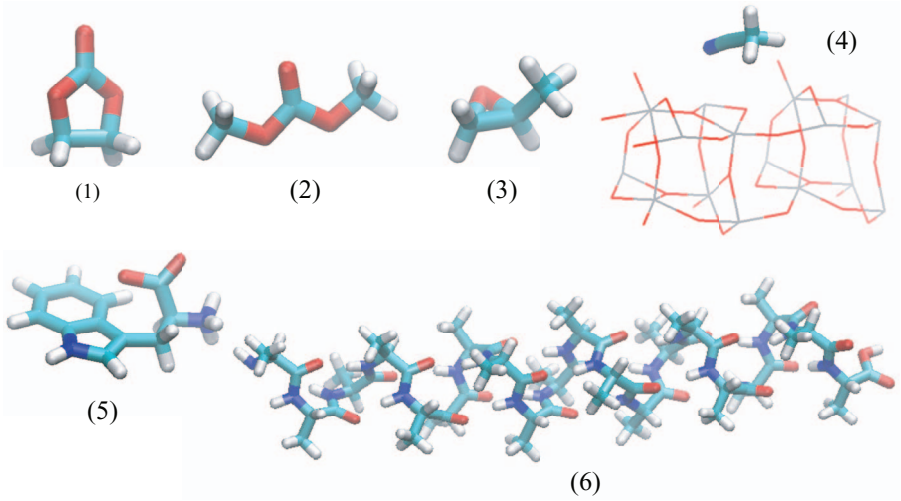

FIG. 1. Molecular structures of EC ["(1)"], DMC ["(2)"], (*S*)-methyloxirane ["(3)"], acetonitrile on a (110) rutile surface ["(4)"], *L*-tryptophan ["(5)"], and α-helical $(Ala)_{20}$ ["(6)"].

evaluation of local electric dipoles of periodic systems yet (for a recent review about fragmentation methods, we refer to Ref. 88). Besides that, other approaches, for instance, the local-field scheme have been proposed and applied to the calculation of molecular crystals.[89–92]

The paper is organized as follows: after the presentation of the theoretical background and computational methodology in Secs. II and III, respectively, the performance of our approach for the calculation of subsystem electric dipole moments is investigated in Sec. IV. The basis set and functional dependence of the computed molecular electric dipole moments is examined in Sec. V. As final test cases in Sec. VI, we investigate IR spectra of ethylene carbonate (EC) and dimethyl carbonate (DMC) (for molecular structures, see Fig. 1), which are frequently used in Lithium ion batteries. A conclusion and outlook can be found in Sec. VII.

II. THEORETICAL BACKGROUND

A. Subsystem DFT-based embedding

In subsystem DFT-based embedding, the total electronic density $\rho(\mathbf{r})$ is separated into subsystem electronic densities $\rho_U(\mathbf{r})$,

$$\rho(\mathbf{r}) = \sum_U \rho_U(\mathbf{r}), \tag{1}$$

where the sum runs over the number of subsystems U. Within KS-DFT, the electronic density of subsystem U is obtained as

$$\rho_U = \sum_i f_{U,i} |\psi_{U,i}|^2. \tag{2}$$

The sum goes over the number of KS orbitals $\{|\psi_{U,i}\rangle\}$ of subsystem U with corresponding occupation numbers $f_{U,i}$ (for sake of brevity, we mostly skip the coordinate dependence of the electronic densities and KS orbitals).

The electronic energy of the whole system under study can be calculated with the (computationally cheaper) HK ansatz

$$E_{\mathrm{HK}}[\rho] = T_{\mathrm{s}}[\rho] + E_{\mathrm{ext}}[\rho] + E_{\mathrm{coul}}[\rho] + E_{\mathrm{xc}}[\rho] \tag{3}$$

with the exchange–correlation functional $E_{\mathrm{xc}}[\rho]$. $T_{\mathrm{s}}[\rho]$ is the non-interacting KE (density) functional and $E_{\mathrm{coul}}[\rho]$ is the Coulomb energy. The interaction energy of the electronic energy with the external potential is given by $E_{\mathrm{ext}}[\rho]$.

The electronic energies within the KS framework are given by

$$E_{\mathrm{KS}}[\rho[\{|\psi_i\rangle\}]] = T_{\mathrm{s}}[\{|\psi_i\rangle\}] + E_{\mathrm{ext}}[\rho] + E_{\mathrm{coul}}[\rho] + E_{\mathrm{xc}}[\rho]. \tag{4}$$

$T_{\mathrm{s}}[\{|\psi_i\rangle\}]$ is the KE (orbital) functional of the non-interacting KS reference system.

Calculating the electronic energy of the whole system under study with the (computationally cheaper) HK ansatz and the subsystem electronic energies within the KS-framework results in[52]

$$\begin{aligned} &E_{\mathrm{emb}}[\rho, \rho_U[\{|\psi_{U,i}\rangle\}]] \\ &= E_{\mathrm{HK}}[\rho] + \sum_U (E_{\mathrm{KS}}[\rho_U[\{|\psi_{U,i}\rangle\}]] - E_{\mathrm{HK}}[\rho_U]) \\ &= T_{\mathrm{s}}[\rho] + E_{\mathrm{coul}}[\rho] + E_{\mathrm{xc}}[\rho] + E_{\mathrm{ext}}[\rho] \\ &\quad + \sum_U (T_{\mathrm{s}}[\{|\psi_{U,i}\rangle\}] - T_{\mathrm{s}}[\rho_U]). \end{aligned} \tag{5}$$

We employ the Gaussian and plane wave method (GPW),[93,94] which naturally includes periodic boundary conditions by expanding the electronic density in plane waves. Furthermore, norm-conserving, separable, dual-space pseudopotentials for the nuclei are employed with a potential consisting of a local part, $V_{\mathrm{loc}}(\mathbf{r})$, and a non-local part, $V_{\mathrm{nonloc}}(\mathbf{r}, \mathbf{r}')$. For a computationally efficient method, $E_{\mathrm{ext}}[\rho]$ is approximated by restricting the interaction of the subsystem electronic densities with the pseudopotentials to the

short-range interaction only[45,52]

$$E_{\text{ext}}[\rho] = \int V_{\text{loc}}(\mathbf{r})\rho(\mathbf{r})\mathrm{d}^3\mathbf{r} + \sum_U \sum_i f_{U,i} \times \langle \psi_{U,i}(\mathbf{r})|V_{\text{U,nonloc}}(\mathbf{r},\mathbf{r}')|\psi_{U,i}(\mathbf{r}')\rangle. \quad (6)$$

Moreover, the KS orbitals of a certain subsystem are solely built from Gaussian basis functions localized on atoms belonging to said subsystem (orthogonality of KS orbitals from different subsets is not enforced). This leads to a strictly block-diagonal KS matrix and is linear scaling with respect to the number of subsets. The KS orbitals of subsystem U can be determined from the coupled KS equations,

$$\left(-\frac{\hbar^2\nabla^2}{2m_e} + V_{\text{KS}}[\rho] + V_{\text{emb}}[\rho,\rho_U]\right)|\psi_{U,i}\rangle = \epsilon_{U,i}\sum_l S_{il}^U|\psi_{U,l}\rangle \quad (7)$$

with the KS potential $V_{\text{KS}}[\rho] = V_{\text{ext}}[\rho] + V_{\text{coul}}[\rho] + V_{\text{xc}}[\rho]$ and the embedding potential

$$V_{\text{emb}}[\rho,\rho_U] = \left.\frac{\delta T_{\text{s}}[\rho]}{\delta\rho}\right|_{\rho} - \left.\frac{\delta T_{\text{s}}[\rho]}{\delta\rho}\right|_{\rho_U}. \quad (8)$$

S_{il}^U is the overlap matrix built of KS orbitals $|\psi_{U,i}\rangle$ and $|\psi_{U,l}\rangle$, m_e the electronic mass, and $\hbar$ Planck's constant divided by 2π.

For generalization encompassing hybrid functionals, we split $E_{\text{xc}}[\rho]$ into an exchange ($E_{\text{x}}[\rho]$) and correlation ($E_{\text{c}}[\rho]$) part. Including exact exchange energy $E_{\text{ex}}[\{|\psi_i\rangle\}]$ into the KS electronic energy expression given in Eq. (4) results in

$$E_{\text{KS}}^{\text{ex}}[\rho[\{|\psi_i\rangle\}]] = T_{\text{s}}[\{|\psi_i\rangle\}] + E_{\text{ext}}[\rho] + E_{\text{coul}}[\rho] + (1-\alpha)E_{\text{x}}[\rho] + \alpha E_{\text{ex}}[\{|\psi_i\rangle\}] + E_{\text{c}}[\rho] \quad (9)$$

with $0 \le \alpha \le 1$. It is common to employ the same exchange–correlation functional $E_{\text{xc}}[\rho]$ in the hybrid and non-hybrid case.

One obtains for the total electronic energy,

$$\begin{aligned} E_{\text{emb}}^{\text{Hybrid}}[\rho,\rho_U[\{|\psi_{U,i}\rangle\}]] &= T_{\text{s}}[\rho] + E_{\text{ext}}[\rho] + E_{\text{coul}}[\rho] + E_{\text{x}}[\rho] + E_{\text{c}}[\rho] \\ &+ \sum_U (T_{\text{s}}[\{|\psi_{U,i}\rangle\}] + E_{\text{c}}[\rho_U] + (1-\alpha)E_{\text{x}}[\rho_U] \\ &+ \alpha E_{\text{ex}}[\{|\psi_{U,i}\rangle\}] \\ &- T_{\text{s}}[\rho_U] - E_{\text{c}}[\rho_U] - E_{\text{x}}[\rho_U]). \end{aligned} \quad (10)$$

Such a line of approach was also suggested in Ref. 68 based on a derivation via the generalized Kohn–Sham scheme.[95]

In contrast to Ref. 68, we additionally use the linear approximation $E_{\text{x}}[\rho] \approx \sum_U E_{\text{x}}[\rho_U]$ in our calculations that simplifies Eq. (10) to

$$\begin{aligned} E_{\text{emb}}^{\text{Hybrid}}[\rho,\rho_U[\{|\psi_{U,i}\rangle\}]] &= T_{\text{s}}[\rho] + E_{\text{ext}}[\rho] + E_{\text{coul}}[\rho] + E_{\text{c}}[\rho] + (1-\alpha)E_{\text{x}}[\rho] \\ &+ \sum_U \alpha E_{\text{ex}}[\{|\psi_{U,i}\rangle\}] + \sum_U (T_{\text{s}}[\{|\psi_{U,i}\rangle\}] - T_{\text{s}}[\rho_U]). \end{aligned} \quad (11)$$

The non-local exact exchange operator is calculated for the subsystems whereas a local exchange operator is evaluated for the total system. This is a practical and efficient approximation avoiding the calculation of non-local exact exchange for the total system, which is in general not available in the subsystem DFT embedding approach. Furthermore, it is still linear scaling with respect to the number of subsystems.

In our implementation, all subsystems are optimized simultaneously and their number is not limited to two subsystems. This is in contrast to the "freeze-and-thaw" approach,[96] where one subsystem electronic density is optimized while the electronic density of the other subsystem(s) is kept frozen.

B. Local electric dipole moments for periodic systems

Given a nonperiodic system containing N electrons, the α component of the electronic part of the electric dipole moment is in general evaluated as

$$d_\alpha^{\text{nonper}} = -e\langle\Phi|R_\alpha|\Phi\rangle = -e\int r_\alpha\rho(\boldsymbol{r})\mathrm{d}^3\boldsymbol{r}, \quad (12)$$

where e is the elementary charge, and α refers to one of the Cartesian (x/y/z) directions. $R_\alpha = \sum_{i=1}^N r_{\alpha,i}$ is given as the sum of the position operators $r_{\alpha,i}$, which can be rewritten as a sum of N identical *one-electron* operators r_α depending each only on one electronic coordinate. $|\Phi\rangle$ is the (N-electron) square-integrable wave function, which goes to zero outside a bounded region in space, and $\rho(\mathbf{r})$ is the corresponding electronic density bounded in space.

Going to the case of non-interacting electrons assumed in KS-DFT, $|\Phi\rangle$ is given by a Slater determinant built from KS orbitals. Employing atom-centered basis functions, KS orbitals can furthermore be written as linear combinations of atomic basis functions $\{|\chi_\nu\rangle\}$, i.e., $|\psi_k\rangle = \sum_\nu C_{\nu k}|\chi_\nu\rangle$, with the expansion coefficients $\{C_{\nu k}\}$. The electronic part of the electric dipole moment can then be calculated via

$$d_\alpha^{\text{nonper}} = -e\sum_i f_i\langle\psi_i|r_\alpha|\psi_i\rangle = -e\sum_{\mu,\nu}(P_{\nu\mu}\langle\chi_\mu|r_\alpha|\chi_\nu\rangle) \quad (13)$$

with the density matrix $P_{\nu\mu} = \sum_i f_i C_{\nu i} C_{\mu i}^\dagger$.

Within periodic boundary conditions, the situation is more involved since the position operator R_α is ill-defined. This problem has been solved by the modern theory of polarization:[14–16] based on a Berry phase,[97] the electronic part of the polarization is obtained as a gauge-invariant phase of the electronic wave function. In the special case of solely one supercell, which is taken to be large in order to

approximate the thermodynamic limit of a system of infinite size, the macroscopic polarization can be expressed as an expectation value of an operator.[98] Considering such a large cubic periodic cell with side length L and taking the Γ point of the Brillouin zone only, the α component of the electronic electric-dipole moment for an insulator in a vanishing macroscopic electric field is as a good approximation given by

$$d_\alpha = -\frac{eL}{2\pi}\mathrm{Im}\ln\langle\Psi|\exp\left\{\mathrm{i}\frac{2\pi}{L}R_\alpha\right\}|\Psi\rangle \tag{14}$$

with the non-degenerate (N-electron) wave function $|\Psi\rangle$. d_α is defined modulo eL. The operator $\exp\{\mathrm{i}\frac{2\pi}{L}R_\alpha\}$ is a *many-electron* operator (except the special case of a system containing only one electron). In contrast to that, R_α in Eq. (12) is a one-electron operator.

Rewriting $|\Psi\rangle$ as a Slater determinant built from KS orbitals leads to the electronic electric dipole moment for non-interacting electrons,[99]

$$d_\alpha = f_{\mathrm{occ}}\frac{eL}{2\pi}\mathrm{Im}\ln\det\boldsymbol{S}_\alpha, \tag{15}$$

with the matrix elements

$$S_{\alpha,kl} = \langle\psi_k|\exp\left\{-\mathrm{i}\frac{2\pi}{L}r_\alpha\right\}|\psi_l\rangle. \tag{16}$$

The indices k and l run over the number of occupied KS orbitals and a same occupation number f_{occ} for all KS orbitals is assumed for simplicity. Analogous expressions for supercells with arbitrary symmetry can be found in Ref. 100.

In the absence of a macroscopic (electric) field, the lowest energy ground state of an infinite insulating system is well defined and solely determined by the ground state electronic density that defines the ground state wave function and thus the electronic macroscopic polarization.[38,101] In contrary, the original HK proof[38] cannot be applied to an infinite insulator in a macroscopic electric field[102] since the energy is not bounded from below. As a consequence, it does not allow for a defined ground state solution. In this case, the macroscopic electronic polarization has to be considered in addition to the electronic density in order to determine the electronic energy of the system. This led to the suggestion of a density-polarization functional theory where said energy is specified by the periodic electronic density and the macroscopic electronic polarization.[102] As a further consequence, the exchange–correlation energy in KS-DFT in principle depends both on the electronic density and on the macroscopic polarization,[103–107] which requires a modification of the KS equations for any insulator with non-zero macroscopic polarization, no matter whether or not a macroscopic electric field is present. However, standard calculations employing exchange–correlation density functionals based on the local density approximation (LDA) or generalized gradient approximation (GGA) do not account for this fact.

For a detailed analysis of the system under study, it is highly desirable to divide the total electric dipole moment of the cell into local electric dipole moments. This is straightforward for the nuclear part of the electric dipole moment but not for the electronic part. The exact splitting into local parts requires the simultaneous diagonalization of the three S_α matrices so that the determinant in Eq. (15) could be rewritten as a product. This is, however, not possible in general. Therefore, a transformation to the KS orbitals can be applied that leads to the best compromise in diagonalizing the three S_α matrices simultaneously leading to the MLWFs,[21,22]

$$|\tilde{\psi}_l\rangle = \sum_i U_{li}|\psi_i\rangle. \tag{17}$$

Commonly, one employs the condition that the second moment (spread) of these functions is minimized (for a recent review, we refer to Ref. 108).

Assuming non-interacting electrons, the electronic contribution to the α component of the electric dipole moment for subset U is then evaluated (modulo eL) as

$$d_\alpha^{U,\mathrm{WC}} = -ef_{\mathrm{occ}}\sum_{l\in U} r_{\alpha,l}^{\mathrm{WC}} = -ef_{\mathrm{occ}}\sum_{l\in U}\left(-\frac{L}{2\pi}\mathrm{Im}\ln s_{\alpha,l}\right) \tag{18}$$

with

$$s_{\alpha,l} = \langle\tilde{\psi}_l|\exp\left\{-\mathrm{i}\frac{2\pi}{L}r_\alpha\right\}|\tilde{\psi}_l\rangle. \tag{19}$$

$\boldsymbol{r}_l^{\mathrm{WC}}$ are the so-called Wannier centers.

Within the embedding approach using atomic-centered basis functions as described above, there is no necessity to apply any localization transformation. This subsystem DFT-based scheme naturally provides well-defined (local) subsets of the system under study. Substituting the KS orbitals $\{|\psi_{U,i}\rangle\}$ of subsystem U into Eq. (15) derived for a periodic system with a KS Slater determinant, one obtains

$$\tilde{d}_\alpha^U = f_{\mathrm{occ}}\frac{eL}{2\pi}\mathrm{Im}\ln\det\boldsymbol{S}_\alpha^U, \tag{20}$$

$$S_{\alpha,kl}^U = \langle\psi_{U,k}|\exp\left\{-\mathrm{i}\frac{2\pi}{L}r_\alpha\right\}|\psi_{U,l}\rangle. \tag{21}$$

Applying $\ln\det\boldsymbol{S}_\alpha^U = \mathrm{Tr}\ln\boldsymbol{S}_{\alpha,kl}^U$, and expanding the matrix elements

$$S_{\alpha,kl}^U \approx 1 - \mathrm{i}\frac{2\pi}{L}\langle\psi_{U,k}|r_\alpha|\psi_{U,l}\rangle \tag{22}$$

as well as the logarithm results in

$$\begin{aligned}\tilde{d}_\alpha^U &\approx -f_{\mathrm{occ}}\frac{eL}{2\pi}\mathrm{Im}\left\{\mathrm{i}\frac{2\pi}{L}\sum_i\langle\psi_{U,i}|r_\alpha|\psi_{U,i}\rangle\right\}\\ &= -f_{\mathrm{occ}}\frac{eL}{2\pi}\mathrm{Im}\left\{\mathrm{i}\frac{2\pi}{L}\sum_i\sum_{\nu,\mu\in U}C_{\nu,i}C_{\mu,i}^\dagger\langle\chi_\mu|r_\alpha|\chi_\nu\rangle\right\}\\ &= -e\sum\nolimits_{\nu,\mu\in U}(P_{\nu\mu}\langle\chi_\mu|r_\alpha|\chi_\nu\rangle)\\ &= -e\int r_\alpha\rho_U(\boldsymbol{r})\mathrm{d}^3\boldsymbol{r}\\ &= d_\alpha^{U,\mathrm{nonper}}.\end{aligned} \tag{23}$$

To first order in $1/L$, the electronic electric dipole moment of subsystem U for that certain branch of the logarithm thus coincides with the one of subsystem U in the nonperiodic case. This is the case since the matrix element given in Eq. (22) is expanded with respect to $1/L$, i.e., the side length L has to be so large that the density matrix and electronic density of subsystem U do not change with L. In this way, the many-electron operator $\exp\{-\mathrm{i}\frac{2\pi}{L}R_\alpha\}$ becomes a one-electron operator as in the non-periodic case.

This is also found starting from Eq. (14): employing the wave function of subsystem U, $|\Psi^U\rangle$, leads to

$$\begin{aligned}\tilde{d}_\alpha^U &= -\frac{eL}{2\pi}\mathrm{Im}\ln\langle\Psi^U|\exp\left\{\mathrm{i}\frac{2\pi}{L}R_\alpha\right\}|\Psi^U\rangle \\ &\approx -\frac{eL}{2\pi}\mathrm{Im}\left\{\mathrm{i}\frac{2\pi}{L}\langle\Psi^U|R_\alpha|\Psi^U\rangle\right\} \\ &= -e\sum\nolimits_{\nu,\mu\in U}(P_{\nu\mu}\langle\chi_\mu|r_\alpha|\chi_\nu\rangle) \\ &= -e\int r_\alpha\rho_U(\boldsymbol{r})\mathrm{d}^3\boldsymbol{r} \\ &= d_\alpha^{U,\mathrm{nonper}}. \end{aligned} \tag{24}$$

Taking Born–von Karman boundary conditions into account, we thus define the α component of the electronic electric dipole moment for the periodic subsystem U as

$$d_\alpha^U = \frac{eL}{2\pi}\mathrm{Im}\ln\exp\left\{-\mathrm{i}\frac{2\pi}{L}\sum\nolimits_{\lambda,\nu\in U}(P_{\lambda\nu}\langle\chi_\nu|r_\alpha|\chi_\lambda\rangle)\right\}, \tag{25}$$

whereby the origin of the electric dipole moment is set to be located in subset U (in this work, the center of charge of the subset under consideration was chosen). d_α^U, defined modulo eL, is gauge invariant, i.e., invariant with respect to unitary transformations of the KS orbitals between themselves. Translational invariance is ensured by choosing neutral, i.e., not charged, subsystems.

The crucial point in our approach is that the size of subsystem U allows the expansion with respect to $1/L$ so that only matrix elements of the one-electron operator r_α have to be calculated. The latter can, within KS-DFT, be rewritten involving the one-body density matrix, i.e., they can in principle be evaluated solely with the help of the subsystem electronic density. This electronic density is, according to the KS theorem,[37] equal to the electronic density of a real interacting system. Nevertheless, the corresponding electric dipole moment represents the one for non-interacting electrons since it is determined by the phase of the wave function, i.e., the KS Slater determinant, which can be expressed by the one-body density matrix due to the assumption of non-interacting electrons. For this non-interacting case, however, the electronic electric dipole moment in Eq. (25) is in principle *exact* for a given subsystem electronic density within the embedding approach (as long as the expansion in Eq. (23) is applicable). In contrast to that, the one from MLWFs is additionally affected by approximations made in the diagonalization and localization procedures [compare Eq. (18)].

We will refer to electric dipole moments obtained employing Eq. (25) within the embedding approach as "Loc-Dip" in the following. Electric dipole moments calculated with the help of Eq. (18) will be termed "WC-Dip(E)" and "WC-Dip(nE)" whereby "(E)" differentiates the ones computed with the embedding approach from the ones evaluated without embedding ["(nE)"].

A bit in the spirit of the above-mentioned Wannier centers, a center of electronic charge for subset U can furthermore be defined as follows:

$$\boldsymbol{r}_{\mathrm{charge}}^U = \frac{\boldsymbol{d}^U}{-e\sum_{\nu,\lambda\in U}(P_{\lambda\nu}\langle\chi_\nu|\chi_\lambda\rangle)}. \tag{26}$$

This is helpful in monitoring changes in the electronic structure, e.g., during dynamic processes.

Subsystem-DFT based embedding has been shown to perform very well for hydrogen-bonded systems[42,43,54,109,110] and van-der-Waals complexes.[48,54,56,111–114] Several deficiencies have been detected in case of subsystems connected with bonds of covalent character.[56,115] In order to avoid this shortcoming, we focus in this work on subsets containing complete molecules and not on subsystems containing molecular fragments.

For the latter, electric dipole moments can still be evaluated for a certain choice of the electric dipole origin since we employ atomic-centered basis functions in the calculations. This allows the definition (modulo eL) of an atomic electronic electric dipole moment for a certain atom B within a given subset (using the same electric dipole moment origin as the one of the molecular electric dipole moment of the corresponding subset),

$$\begin{aligned} d_\alpha^B &= d_\alpha^{B,\mathrm{intra}} + d_\alpha^{B,\mathrm{inter}} \\ &= \frac{eL}{2\pi}\mathrm{Im}\ln\exp\left\{-\mathrm{i}\frac{2\pi}{L}\left(\sum_{\gamma,\nu\in B}P_{\nu\gamma}\langle\chi_\gamma|\boldsymbol{r}_\alpha|\chi_\nu\rangle\right)\right\} \\ &\quad + \frac{eL}{2\pi}\mathrm{Im}\ln\exp\left\{-\mathrm{i}\frac{2\pi}{L}\left(\sum_{\gamma\in B}\sum_{\nu\notin B}P_{\nu\gamma}\langle\chi_\gamma|\boldsymbol{r}_\alpha|\chi_\nu\rangle\right)\right\}. \end{aligned} \tag{27}$$

III. COMPUTATIONAL METHODOLOGY

We implemented the calculation of subset/atomic electric dipole moments employing the embedding approach into the QUICKSTEP module[52,94] of the CP2K program package.[116] DFT in the framework of the GPW method was used in all calculations. The kinetic energy cutoff for the plane wave expansion was set to 280 Ry. If not mentioned otherwise, Goedecker–Teter–Hutter (GTH) pseudopotentials[117–119] and the corresponding TZVP-GTH basis sets were employed. Furthermore, the BLYP[120,121] exchange–correlation functional was chosen and the LLP kinetic energy functional[122] in case of embedding. MLWFs with the Berry phase approach were computed employing the standard settings as implemented in CP2K (i.e., a tolerance of 10^{-5} for the convergence criterion of the Jacobi localization method). Tighter criteria did not have any noticeable influence on the electric dipole moment values.

IR spectra shown in Sec. VI were obtained from Born–Oppenheimer MD simulations with DFT as the electronic structure method. The propagation time step in the MD runs was set to 0.4 fs. Grimme's D3 dispersion correction[123] was applied in order to account for van der Waals interactions. For liquid EC, a cubic periodic box containing 15 EC molecules was taken with a density of 1.32 kg/l as found in experiment.[124] For the mixture of EC and DMC, seven molecules of both EC and DMC were chosen in a cubic box with a side length of 12.028 Å. Since the cis–cis conformer of DMC has been found to be the most stable one,[125] we included four cis–cis and three cis–trans conformers into the simulation cell. The systems were equilibrated in the *NVT* ensemble for 5 ps at a temperature of 320 K (EC) and 298.5 K (EC/DMC), respectively, using KS-DFT and a Nosé–Hoover chain thermostat.[126,127] The production runs were performed in the *NVE* ensemble with KS-DFT for 20 ps (15 ps in the case of a single EC molecule). From these trajectories, molecular electric dipole moments (with or without embedding) were afterwards calculated as a postprocessing step whereby the electric dipole moments were calculated for each fifth step. The spectra were plotted with the help of a modified version of the program TRAVIS[30,128] applying zero padding and a Hanning type window function. The IR intensities were multiplied by the harmonic approximation quantum correction factor $\frac{(\hbar\omega/kT)}{1-\exp(-\hbar\omega/kT)}$ where ω is the angular frequency, k Boltzmann's constant, and T the temperature (for details, see Ref. 129). For all electric dipole moments reported in this paper, the origin was set to the center of atomic charge of the subsystem under consideration. This is also true for atomic electric dipole moments computed according to Eq. (27) where the origin was set to the center of atomic charge of the subsystem containing the atom of interest. In an analogous manner, the systems presented in Sec. IV were propagated with KS-DFT based Born–Oppenheimer MD for 1 ps whereby the propagation time step was set to 0.5 fs. Electric dipole moments from MLWFs were evaluated at every 2.5 fs. These trajectories were afterwards used to calculate electric dipole moments within the embedding approximation for every fifth step.

IV. VALIDATION OF THE METHODOLOGY

In order to test the computation of electric dipole moments evaluated according to Eq. (25), we studied several systems.

A. Liquids

The first system under study was liquid EC modelled by 15 EC molecules in a periodic box (compare Sec. III). Each EC molecule was chosen as a subset in the embedding calculation. For comparison, electric dipole moments were obtained from MLWFs within the embedding scheme. Mean relative differences were calculated as

$$\Delta^{\mathrm{WC/Loc}} = \frac{1}{3} N_{\mathrm{subset}}^{-1} N_{\mathrm{snap}}^{-1} \left[\sum_{\alpha=1}^{3} \sum_{a}^{N_{\mathrm{subset}}} \sum_{b}^{N_{\mathrm{snap}}} \left| \frac{d_\alpha^{a,b,\mathrm{WC}} - d_\alpha^{a,b}}{d_\alpha^{a,b}} \right| \right], \tag{28}$$

where N_{subset} is the number of subsets and N_{snap} the number of snapshots considered (absolute values of 0.20 D or lower were discarded in the calculation of relative differences). These mean relative differences were small: on average 2.1%, 1.9%, and 2.5% for the electric dipole moments in x-, y-, and z-direction, respectively (mean standard deviation (mSD): 2.3%). In order to get an impression of the influence of the embedding approach compared to a standard KS calculation, electric dipole moments from MLWFs were computed without embedding as well. Corresponding mean relative differences were evaluated as

$$\Delta^{\mathrm{Loc/WC-nE}} = \frac{1}{3} N_{\mathrm{subset}}^{-1} N_{\mathrm{snap}}^{-1} \left[\sum_{\alpha=1}^{3} \sum_{a}^{N_{\mathrm{subset}}} \sum_{b}^{N_{\mathrm{snap}}} \left| \frac{d_\alpha^{a,b} - d_\alpha^{a,b,\mathrm{WC-nE}}}{d_\alpha^{a,b,\mathrm{WC-nE}}} \right| \right]. \tag{29}$$

A comparable mean relative difference was found [2.1% on average (mSD: 2.1%)]. In contrast to that, the difference between the MLWFs obtained with and without embedding was tiny. This can be seen in the mean relative difference (on average 0.1%) between WC-Dip(E) and WC-Dip(nE) calculated via

$$\Delta^{\mathrm{WC/WC-nE}} = \frac{1}{3} N_{\mathrm{subset}}^{-1} N_{\mathrm{snap}}^{-1} \left[\sum_{\alpha=1}^{3} \sum_{a}^{N_{\mathrm{subset}}} \sum_{b}^{N_{\mathrm{snap}}} \left| \frac{d_\alpha^{a,b,\mathrm{WC}} - d_\alpha^{a,b,\mathrm{WC-nE}}}{d_\alpha^{a,b,\mathrm{WC-nE}}} \right| \right]. \tag{30}$$

This difference arises from the approximations introduced by the embedding approach and the determination of the MLWFs.

In the same way, the molecular electric dipole moments of a mixture of EC and DMC (see Sec. III) were computed. The electric dipole moments calculated according to Eq. (25) and the ones computed from MLWFs were similar giving rise to 3.1% for $\Delta^{\mathrm{WC/Loc}}$ (mSD: 4.0%). Considering the impact of the embedding resulted in a slightly higher $\Delta^{\mathrm{Loc/WC-nE}}$ value of 3.4% (mSD: 3.7%). The mean relative difference between the WC-Dips, calculated with and without embedding, was small ($\Delta^{\mathrm{WC/WC-nE}} = 1.9\%$; mSD: 3.0%).

As a third test system, (*S*)-methyloxirane, a commonly used solvent in industry, was investigated (for its molecular structure, see Fig. 1). This liquid was simulated with a periodic cubic box containing 20 subsets of (*S*)-methyloxirane molecules at a density of 0.830 g/l.[130,131] Again, $\Delta^{\mathrm{WC/Loc}}$ was found to be minor, namely, 4.0% (mSD: 2.9%), and $\Delta^{\mathrm{Loc/WC-nE}}$ somewhat larger (5.0%; mSD: 3.5%). The mean relative difference between WC-Dip(E) and WC-Dip(nE) was 2.5% (mSD: 2.9%). Another liquid of outstanding interest is of course water. Using a water box (cubic periodic box with a side length of 9.855 Å) filled with 32 water molecules, a small $\Delta^{\mathrm{WC/Loc}}$ value of 1.7% (mSD: 3.8%) was evaluated.

B. Molecules solvated with water

Going from pure water to a mixed solute/solvent system, we computed the electric dipole moment of α-helical $(Ala)_{20}$[132–134] (see Fig. 1 for the molecular structure), which was located in a periodic cubic cell (side length: 42 Å) and solvated with 424 water molecules. A negligibly small variation between the molecular electric dipole moments obtained with our approach and via MLWFs was calculated for the α-helix (203 atoms): $\Delta^{\mathrm{WC/Loc}}$ was only 0.08%. The additional effect of the embedding was relatively small with 2.9% (2.8%), 0.8% (0.8%), and 6.8% (6.8%) for the x-, y-, and z-components of $\Delta^{\mathrm{Loc/WC\text{-}nE}}$ ($\Delta^{\mathrm{WC/WC\text{-}nE}}$). A similar picture was obtained for the amino acid *L*-tryptophan, whose molecular structure is given in Fig. 1. Employing one molecule surrounded by 90 water molecules in a periodic cubic box with a side length of 11.85 Å, the $\Delta^{\mathrm{WC/Loc}}$ values for the x-, y-, and z-components of the electric dipole moment belonging to the *L*-tryptophan molecule were 1.2%, 1.5%, and 0.6%; considering $\Delta^{\mathrm{Loc/WC\text{-}nE}}$, 5.7%, 1.3%, and 3.3% were obtained. This shows a fortunate error cancellation for the y-component of the electric dipole moment since the ones computed according to Eq. (25) were on average closer to the corresponding WC-Dip(nE) than to the WC-Dip(E). A relatively high deviation was found for the x-component, which to a large part appears to originate from the approximations introduced by the embedding scheme (similar to $\Delta^{\mathrm{WC/WC\text{-}nE}}$ with 6.4%, 2.1%, and 3.8% for the x-, y-, and z-components, respectively).

C. Molecule on surface

Beside the liquid systems considered so far, we investigated an example of a molecule adsorbed on a surface. In more detail, an acetonitrile molecule on a (110) rutile surface was examined (using a monoclinic cell with cell parameters a = 13.028 Å, b = −5.932 Å, c = −9.771 Å, $\alpha = \gamma = 90°$, $\beta = 135°$). The molecule sticks with its nitrogen atom to a titanium atom of the surface, being about 2.52 Å apart from the metal atom (see Fig. 1). Taking acetonitrile as a subset in the electric dipole moment calculation, we found values of 9.6%, 1.8%, and 1.4% for $\Delta^{\mathrm{WC/Loc}}$ in the x-, y-, and z-direction, respectively. Larger was the deviation if additionally the embedding approximation was considered leading to 20.0%, 2.7%, and 13.8% for $\Delta^{\mathrm{WC/WC\text{-}nE}}$ corresponding to the x-, y-, and z-direction, respectively. Thus, in particular the x-component of the electric dipole moment was affected by the embedding and MLWF approximations. This can also be noticed in the deviation of the Loc-Dip values from the WC-Dip(nE) values where the average relative differences were 24.0%, 2.0%, and 14.2%, respectively. Going to larger cell dimensions or employing another KE functional instead of LLP may reduce the embedding error.

V. BASIS SET AND FUNCTIONAL DEPENDENCE

The results presented so far were computed with the TZVP-GTH basis set in combination with the BLYP and LLP density functionals. In order to test the accuracy of our approach with respect to different basis sets, data obtained with distinct basis sets are given in Table I for liquid EC.

TABLE I. Investigation of the basis set, exchange–correlation functional ("ExC fct."), and KE functional ("KE fct.") dependence for liquid EC: mean relative differences obtained from electric dipole moments calculated according to Eq. (25) and from MLWFs computed either with embedding ("$\Delta^{\mathrm{WC/Loc}}$") or without embedding ("$\Delta^{\mathrm{Loc/WC\text{-}nE}}$") (mSD is given in brackets).

Basis set/ExC fct./KE fct.	$\Delta^{\mathrm{WC/Loc}}$ (%)	$\Delta^{\mathrm{Loc/WC\text{-}nE}}$ (%)
SZV-GTH/BLYP/LLP	3.46 (1.65)	6.69 (4.90)
DZVP-GTH/BLYP/LLP	2.38 (3.23)	3.97 (3.09)
TZVP-GTH/BLYP/LLP	2.30 (3.24)	2.77 (3.19)
TZV2P-GTH/BLYP/LLP	2.58 (3.30)	3.12 (3.01)
QZV2P-GTH/BLYP/LLP	2.39 (3.05)	2.51 (2.75)
QZV3P-GTH/BLYP/LLP	2.50 (3.15)	2.63 (2.67)
TZVP-GTH/BP86/LLP	2.43 (3.28)	2.80 (3.25)
TZVP-GTH/PBE/LLP	2.41 (3.23)	2.86 (3.12)
TZVP-GTH/PBE0/LLP	2.01 (3.16)	2.24 (3.00)
TZVP-GTH/BLYP/LP	2.41 (3.36)	2.93 (3.23)
TZVP-GTH/BLYP/TF	2.43 (3.39)	2.90 (3.19)
TZVP-GTH/BLYP/PERDEW	2.34 (3.14)	3.17 (3.39)
TZVP-GTH/BLYP/TW1	2.27 (3.22)	2.66 (3.15)
TZVP-GTH/BLYP/LC94	2.31 (3.25)	2.78 (3.22)
TZVP-GTH/BLYP/PEARSON	2.38 (3.23)	3.08 (3.42)

The basis sets were taken from the CP2K repository (for details, we refer to Ref. 94). The smallest mean deviation of WC-Dip(E) from Loc-Dip was found for the TZVP-GTH basis set with $\Delta^{\mathrm{WC/Loc}} = 2.3\%$ whereas the single-zeta valence (SZV-GTH) basis set gave rise to the highest value of 3.5%. Adding polarization functions to the TZVP-GTH basis set leads to the TZV2P-GTH basis set, which, however, resulted in worse results than TZVP-GTH, both with respect to $\Delta^{\mathrm{WC/Loc}}$ and $\Delta^{\mathrm{Loc/WC\text{-}nE}}$. Going to quadrupole-zeta valence basis sets (QZV2P-GTH, QZV3P-GTH) slightly reduced the error between Loc-Dip and WC-Dip(nE) but did not give smaller $\Delta^{\mathrm{WC/Loc}}$ values.

Another important parameter in DFT calculations is the exchange–correlation density functional. We chose several popular functionals: in addition to the above-mentioned BLYP density functional, two other GGA functionals, namely, BP86[120,135] and PBE,[136,137] were tested as well as the Hybrid–GGA functional PBE0.[136–138] As can be seen in Table I, the BLYP, BP86, and PBE density functionals gave very similar results, both with respect to the comparison of Loc-Dip with WC-Dip(E) and Loc-Dip with WC-Dip(nE). Coming to the hybrid functional PBE0, lower deviations were observed: $\Delta^{\mathrm{WC/Loc}}$ and $\Delta^{\mathrm{Loc/WC\text{-}nE}}$ were solely 2.0% and 2.2%, respectively. (The calculation of the WC-Dip(E) values from the converged wave function took about 5.9 s in case of PBE0 and 6.7 s for PBE, the corresponding Loc-Dip values were calculated in less than 0.01 s.[139]) In order to speed up the calculation of the exact exchange part, we also applied the auxiliary density matrix method (ADMM)[140] in the PBE0 calculation (using the cFit3 auxiliary basis sets[140]). The approximations brought in by the ADMM approach led to an error cancellation reducing $\Delta^{\mathrm{WC/Loc}}$ and $\Delta^{\mathrm{Loc/WC\text{-}nE}}$ to 1.9%

and 1.4% (if a purified wave function fitting was applied) and to 1.9% and 1.6% (if no density matrix purification was employed), respectively. B3LYP brought about a very similar outcome. Thus, the electric dipole moment components computed with MLWFs and no embedding deviated less from the ones calculated according to Eq. (25) than the ones obtained with MLWFs and embedding.

Going to a number of diverse KE density functionals, the LDA-based KE density functionals LP[141] and TF[142,143] performed minimally poorer in the comparison of Loc-Dip vs. WC-Dip(E) (see Table I) than the GGA-based Perdew,[144] TW1,[145] LC94,[146] and Pearson[147,148] KE density functionals. A bit more pronounced was the mismatch between the calculation with and without embedding: whereas the Perdew and Pearson KE density functionals gave rise to a $\Delta^{\text{Loc/WC-nE}}$ value of 3.2% and 3.1%, respectively, the TW1 KE functionals led to a value of 2.7%. The LC94 (often also referred to as PW91) and LLP functionals resulted in slightly higher percentages around 2.8%. The LDA-based LP and TF KE functionals performed moderately (around 2.9%).

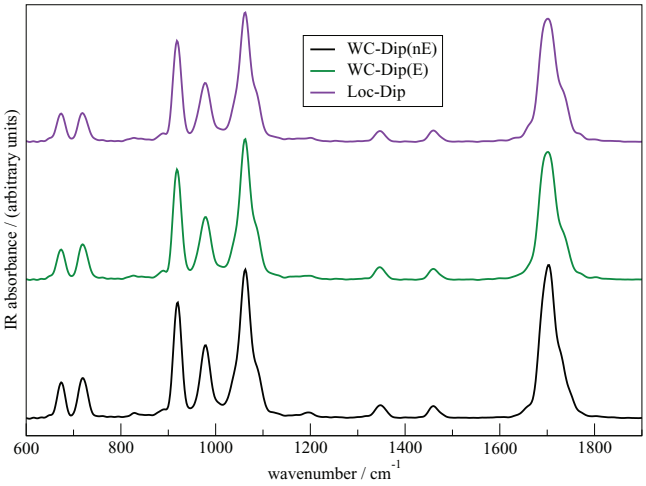

FIG. 2. IR spectra of liquid EC calculated from MD (TZVP-GTH/BLYP; additionally LLP in the embedding calculation) employing molecular electric dipole moments calculated according to Eq. (25) ["Loc-Dip"] (top), from MLWFs with embedding ["WC-Dip(E)"] (middle), and from MLWFs without embedding ["WC-Dip(nE)"] (bottom); for details, see text.

VI. EXAMPLE APPLICATIONS: EC AND DMC

An important component in the development of high-performance batteries is the choice of the electrolyte. Besides the requirements of low toxicity, volatility, and cost, the electrolyte should show good thermal and electrochemical stability combined with high conductivity. Of crucial importance for Lithium ion batteries is the formation of an organic/inorganic layer at the graphite anode/electrolyte interface, the so-called solid-electrolyte interface (SEI).[149–153] It prevents further electron injection into the electrolyte accompanied with electrolyte decomposition as well as exfoliation of the graphene layers whereas Lithium ions can ideally still diffuse through the SEI. The complex mechanism of SEI formation has not been completely understood and numerous experimental and theoretical work has been conducted (for an overview about recent work, we refer to Refs. 152 and 154–158 and references cited therein). EC is often used as a co-solvent in Lithium ion batteries. The advantage of EC is that it decomposes on the electrode surface during the first charging, forming the SEI. This leads to a passivation of the surface and enables the selective migration of Li ions through the SEI. Such a SEI is, for example, not found in case of propylene carbonate as solvent.[151] It is thus important to understand the formation and influence of the SEI, which, however, requires the application of a surface-sensitive method such as certain variants of vibrational spectroscopy.[154,155,159,160] A combination of *in situ* Raman/FT-IR spectroscopy has recently been applied by Novák *et al.* for the characterization of Lithium ion containing electrolytes and their behaviour at glassy carbon electrodes with EC and DMC as solvents.[154]

In order to be able to interpret features in measured IR spectra, it is helpful to differentiate the contributions of the various ingredients. The IR spectrum of liquid EC, for instance, can be computed via MD where the spectrum is accessible through electric dipole moment time autocorrelation functions. Fig. 2 shows the IR spectrum of EC which was obtained by autocorrelation of the sum of the molecular electric dipole moments. The molecular electric dipole moments were computed with the help of Eq. (25) or from MLWFs whereby the latter were determined both with and without embedding. The agreement between all three spectra in Fig. 2 is very good. The only well recognizable difference is the intensity of the doublet centered around 700 cm^{-1} where ring bending vibrations occur:[161] a slightly more intense band at the higher wavenumber side is obtained if MLWFs are employed whereas the two bands show similar intensity in case of the Loc-Dip approach. This makes clear that the evaluation of molecular electric dipole moments as suggested in Eq. (25) is a valuable alternative to the one based on the localization of Wannier functions for this type of liquid. It furthermore demonstrates that the tiny difference between these approaches as discussed in Sec. IV does not affect the overall appearance of the IR spectra of liquid EC.

At ambient conditions, pure EC is not a favorable electrolyte solvent owing to a relatively high melting point (around 309.5 K).[151] A remedy for this is the admixture of linear carbonates. These feature lower melting points and, advantageously, a lower viscosity and dielectric constant leading to a higher ion conductivity. Especially, DMC has been found to be a favourable co-solvent since DMC/EC mixtures are electrochemically stable over a wide range of voltages.[151] The IR spectrum of a 50:50 mixture of EC/DMC (compare Sec. III) is given on the bottom of Fig. 3. In order to trace back the origin of the bands, contributions from the two different kinds of molecules were calculated with the help of molecular electric dipole moments. The second lowest panel shows the IR spectra arising either from the EC or DMC molecules (crosscorrelation contributions are not considered). The spectra obtained from the different approaches are very similar and no noteworthy difference can be seen in the band shapes. As already observed in the spectrum of pure EC, a minor difference in the height of the bands between the Loc-Dip and WC-Dip(E) spectrum is observed for the doublet around 700

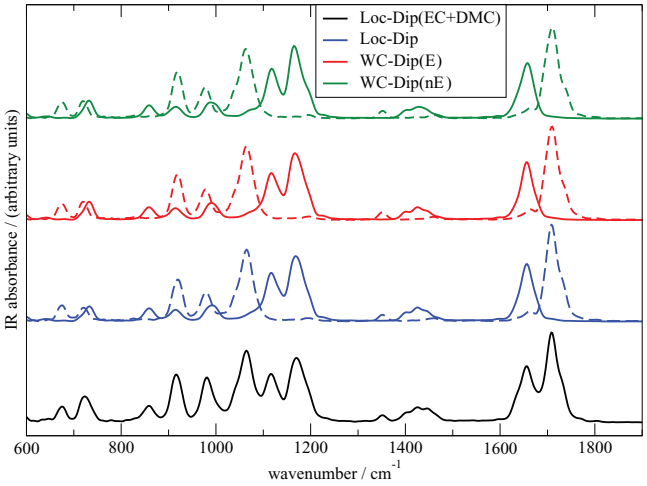

FIG. 3. IR spectra of a mixture of DMC and EC molecules obtained from MD (TZVP-GTH/BLYP; in addition to LLP in the embedding calculation) employing molecular electric dipole moments calculated according to Eq. (25) ["Loc-Dip"] (bottom and second lowest), from MLWFs with embedding ["WC-Dip(E)"] (second highest), and from MLWFs without embedding ["WC-Dip(nE)"] (top); the dashed lines correspond to the spectra obtained from EC molecules and the drawn-through lines show the spectra derived from DMC molecules (except the spectrum at the bottom, which shows the sum of the spectra of the EC and DMC molecules; for details, see text).

cm^{-1}, but otherwise the agreement is very good. Comparing to the spectra obtained from WC-Dip(nE), it is also obvious that the embedding approach does not introduce significant changes except of tiny variations in the height of the bands.

An average of 7.58 D (mSD: 0.48 D) was obtained for the absolute values of the molecular (Loc-Dip) electric dipole moment of an EC molecule in the pure EC liquid. The analogous averages for WC-Dip(E) and WC-Dip(nE) were 7.69 D (mSD: 0.49 D) and 7.74 D (mSD: 0.50 D), respectively. Although the WC-Dip averages were slightly larger, they did not remarkably affect the appearance of the IR bands. The latter were obtained by autocorrelating the electric dipole moment components, which led to an error cancellation. For a single EC molecule in gas phase, an absolute value of 5.65 D was computed. Modelling one EC molecule at ambient conditions via a MD simulation, we found an average absolute value of 5.56 D (mSD: 0.19 D). This is in good agreement with the experimental value of 5.35±0.15 D, which has been determined from Stark-effect measurements.[162] The difference between the gas phase and liquid molecular electric dipole moments can thus primarily be attributed to the interactions introduced by surrounding molecules.

In order to investigate the above-mentioned variations in the EC molecular electric dipole moment in more detail, we calculated the absolute values of its atomic electric dipole moments according to Eq. (27). The atomic electric dipole moment origin was set to the same origin as the one of the corresponding molecular electric dipole moment (i.e., the center of charge of the subsystem). On average, an increase by 31% and 112% was calculated for the oxygen and carbon atom of the carbonyl group, respectively, if the liquid EC values were compared to the one of EC in gas phase. A smaller enhancement in the absolute electric dipole moment values was also obtained for the oxo and hydrogen atoms whereas a quite marginal decrease was computed for the carbon atoms. The atomic electric dipole moments computed following Eq. (27) are, similar to Mulliken atomic charges,[163] rather basis set dependent. Nevertheless, it can be concluded that the increase of the absolute electric dipole moment of a liquid EC molecule compared to the one of a gas phase EC molecule (all obtained with the TZVP-GTH basis set) mostly arises from distinct contributions from its carbonyl group.

VII. CONCLUSION AND OUTLOOK

We presented an efficient approach for the calculation of local electric dipole moments with an emphasis on periodic systems. Within the described subsystem DFT-based embedding scheme encompassing both hybrid and non-hybrid exchange–correlation functionals, subset electric dipole moments can be computed without any extra localization procedure leading to small additional cost in the calculations. Due to the approximations induced by the embedding approach, it is preferably applied to subsystems not connected via covalent bonds, but this can be improved, i.e., by development of more sophisticated KE functionals. It is eminently suited for the study of molecular systems such as liquids, for which the embedding method is known to perform very well.

In contrast to local electric dipole moments from MLWFs, our scheme can straightforward be employed in density-matrix based linear-scaling DFT because no calculation of KS orbitals is necessary. Aside from that, said subset electric dipole moments can be rigorously divided into atomic molecular electric dipoles. This does not require the assignment of a specific number of electrons to each atom as needed in the determination of electric dipole moments from Wannier centers. The electronic distribution is naturally accounted for in our decomposition scheme.

Within the described embedding framework, the subset electric dipole moments employing our approach are exact for a given subsystem electronic density (as long as the expansion according to Eq. (23) is applicable). Opposed to that, the corresponding ones from MLWFs are affected by approximations made in the diagonalization and localization procedures. These electric dipole moments computed from MLWFs with embedding, however, deviated only marginally from the ones derived via our method for the examined subsystems. There are in principle different ways to obtain subsystem electronic densities (see Ref. 164 and references therein). Nevertheless, employing the embedding scheme outlined above, only a small impact of the embedding was observed in most cases, which can be further reduced by choosing improved KE functionals. In accordance to that, we found only a minor dependency on the KE functional in the case of liquid EC.

An excellent agreement between IR spectra calculated with and without MLWFs was obtained for liquid EC and a mixture of DMC/EC, which is commonly used as solvent in Lithium ion batteries. Further analysis showed that the absolute values of the molecular electric dipole moments in liquid EC are remarkably higher compared to the one of a single, isolated EC molecule. This enhancement can mainly be traced back to a larger contribution of the EC carbonyl group

as shown by the decomposition into atomic electric dipole moments.

All in all, the described method for the calculation of local electric dipole moments is a valuable, computationally inexpensive approach for the determination of subset electric dipole moments in (non-)periodic systems, which can be applied in combination with hybrid or non-hybrid exchange–correlation functionals. It can be used, for example, to monitor changes in the electric dipole moment and center of electronic charge of (solvated) molecules or adsorbates on surfaces, which facilitates the interpretation of chemical processes and vibrational spectra. Subset electric dipole moments can furthermore easily be computed by post-processing of any trajectory file. This opens a convenient way to model the dynamics of the system under study and its properties with different settings at reduced computational effort. In addition, our approach can be extended to other local properties that may otherwise be difficult to access, in particular for periodic systems.

ACKNOWLEDGMENTS

The author thanks Professor Jürg Hutter for discussions and continuous support. Generous computing resources from the Swiss National Supercomputing Center (Project ID: s425) are gratefully acknowledged.

[1]R. Car and M. Parrinello, Phys. Rev. Lett. **55**, 2471 (1985).
[2]D. Marx and J. Hutter, *Ab Initio Molecular Dynamics: Basic Theory and Advanced Methods* (Cambridge University Press, Cambridge, 2009).
[3]E. B. Wilson, Jr., J. C. Decius, and P. C. Cross, *Molecular Vibrations* (McGraw-Hill, New York, 1955).
[4]J. Neugebauer, M. Reiher, C. Kind, and B. A. Hess, J. Comput. Chem. **23**, 895 (2002).
[5]S. Luber, C. Herrmann, and M. Reiher, J. Phys. Chem. B **112**, 2218 (2008).
[6]S. Luber and M. Reiher, Chem. Phys. **346**, 212 (2008).
[7]S. Luber, J. Neugebauer, and M. Reiher, J. Chem. Phys. **130**, 064105 (2009).
[8]S. Luber and M. Reiher, J. Phys. Chem. A **113**, 8268 (2009).
[9]S. Luber and M. Reiher, ChemPhysChem **11**, 1876 (2010).
[10]S. Luber and M. Reiher, J. Phys. Chem. B **114**, 1057 (2010).
[11]O. Mohammed, S. Luber, V. S. Batista, and E. T. J. Nibbering, J. Phys. Chem. A **115**, 7550 (2011).
[12]T. Weymuth, M. P. Haag, K. Kiewisch, S. Luber, S. Schenk, C. R. Jacob, C. Herrmann, J. Neugebauer, and M. Reiher, J. Comput. Chem. **33**, 2186 (2012).
[13]S. Luber, K. Adamczyk, E. T. J. Nibbering, and V. S. Batista, J. Phys. Chem. A **117**, 5269 (2013).
[14]R. D. King-Smith and R. Resta, Phys. Rev. B **47**, 1651 (1993).
[15]R. Resta, Europhys. Lett. **22**, 133 (1993).
[16]R. Resta, Rev. Mod. Phys. **66**, 899 (1994).
[17]D. M. Bishop, F. L. Gu, and B. Kirtman, J. Chem. Phys. **114**, 7633 (2001).
[18]D. Jacquemin, J. André, and B. Champagne, J. Chem. Phys. **118**, 3956 (2003).
[19]M. Springborg and B. Kirtman, Phys. Rev. B **77**, 045102 (2008).
[20]L. Maschio, B. Kirtman, R. Orlando, and M. Rérat, J. Chem. Phys. **137**, 204113 (2012).
[21]G. H. Wannier, Phys. Rev. **52**, 191 (1937).
[22]N. Marzari and D. Vanderbilt, Phys. Rev. B **56**, 12847 (1997).
[23]M. Bernasconi, P. Silvestrelli, and M. Parrinello, Phys. Rev. Lett. **81**, 1235 (1998).
[24]P. L. Silvestrelli and M. Parrinello, Phys. Rev. Lett. **82**, 3308 (1999).
[25]M.-P. Gaigeot and M. Sprik, J. Phys. Chem. B **107**, 10344 (2003).
[26]B. Kirchner and J. Hutter, J. Chem. Phys. **121**, 5133 (2004).
[27]M.-P. Gaigeot, R. Vuilleumier, M. Sprik, and D. Borgis, J. Chem. Theory Comput. **1**, 772 (2005).
[28]M.-P. Gaigeot, Phys. Chem. Chem. Phys. **12**, 3336 (2010).
[29]C. Zhang, D. Donadio, F. Gygi, and G. Galli, J. Chem. Theory Comput. **7**, 1443 (2011).
[30]M. Thomas, M. Brehm, R. Fligg, P. Vöhringer, and B. Kirchner, Phys. Chem. Chem. Phys. **15**, 6608 (2013).
[31]R. G. Gordon and Y. S. Kim, J. Chem. Phys. **56**, 3122 (1972).
[32]Y. S. Kim and R. G. Gordon, J. Chem. Phys. **60**, 1842 (1974).
[33]G. Senatore and K. R. Subbaswamy, Phys. Rev. B **34**, 5754 (1986).
[34]P. Cortona, Phys. Rev. B **44**, 8454 (1991).
[35]T. A. Wesolowski and A. Warshel, J. Phys. Chem. **97**, 8050 (1993).
[36]M. E. Casida and T. A. Wesolowski, J. Quantum Chem. **96**, 577 (2004).
[37]W. Kohn and L. J. Sham, Phys. Rev. **140**, A1133 (1965).
[38]P. Hohenberg and W. Kohn, Phys. Rev. **136**, B864 (1964).
[39]T. A. Wesolowski, J. Phys. A **36**, 10607 (2003).
[40]T. A. Wesolowski, "One-electron equations for embedded electron density: Challenge for theory and practical payoffs in multi-level modeling of complex polyatomic systems," in *Computational Chemistry: Reviews of Current Trends*, edited by J. Leszcynski (World Scientific, Singapore, 2006), Vol. 10, pp. 1–82.
[41]O. V. Gritsenko and L. Visscher, Phys. Rev. A **82**, 032519 (2010).
[42]T. Wesolowski, H. Chermette, and J. Weber, J. Chem. Phys. **105**, 9182 (1996).
[43]T. Wesolowski, J. Chem. Phys. **106**, 8516 (1997).
[44]E. Stefanovich and T. Truong, J. Chem. Phys. **104**, 2946 (1996).
[45]J. Trail and D. Bird, Phys. Rev. B **62**, 16402 (2000).
[46]T. Wesolowski, A. Goursot, and J. Weber, J. Chem. Phys. **115**, 4791 (2001).
[47]C. R. Jacob, J. Neugebauer, L. Jensen, and L. Visscher, Phys. Chem. Chem. Phys. **8**, 2349 (2006).
[48]C. Jacob, T. Wesolowski, and L. Visscher, J. Chem. Phys. **123**, 174104 (2005).
[49]J. Neugebauer, M. J. Louwerse, E. J. Baerends, and T. A. Wesolowski, J. Chem. Phys. **122**, 094115 (2005).
[50]J. Neugebauer, M. Louwerse, P. Belanzoni, T. Wesolowski, and E. Baerends, J. Chem. Phys. **123**, 114101 (2005).
[51]C. R. Jacob and L. Visscher, J. Chem. Phys. **125**, 194104 (2006).
[52]M. Iannuzzi, B. Kirchner, and J. Hutter, Chem. Phys. Lett. **421**, 16 (2006).
[53]C. R. Jacob, J. Neugebauer, and L. Visscher, J. Comput. Chem. **29**, 1011 (2008).
[54]K. Kiewisch, G. Eickerling, M. Reiher, and J. Neugebauer, J. Chem. Phys. **128**, 044114 (2008).
[55]J. Neugebauer and E. J. Baerends, J. Phys. Chem. A **110**, 8786 (2006).
[56]S. Fux, K. Kiewisch, C. R. Jacob, J. Neugebauer, and M. Reiher, Chem. Phys. Lett. **461**, 353 (2008).
[57]R. E. Bulo, C. R. Jacob, and L. Visscher, J. Phys. Chem. A **112**, 2640 (2008).
[58]J. D. Goodpaster, T. A. Barnes, and T. F. Miller III, J. Chem. Phys. **134**, 164108 (2011).
[59]S. Höfener, A. S. P. Gomes, and L. Visscher, J. Chem. Phys. **136**, 044104 (2012).
[60]S. Laricchia, E. Fabiano, and F. Della Sala, J. Chem. Phys. **137**, 014102 (2012).
[61]A. S. P. Gomes, C. R. Jacob, F. Real, L. Visscher, and V. Vallet, Phys. Chem. Chem. Phys. **15**, 15153 (2013).
[62]T. Klüner, N. Govind, Y. A. Wang, and E. A. Carter, Phys. Rev. Lett. **86**, 5954 (2001).
[63]J. Neugebauer, J. Chem. Phys. **126**, 134116 (2007).
[64]A. S. P. Gomes, C. R. Jacob, and L. Visscher, Phys. Chem. Chem. Phys. **10**, 5353 (2008).
[65]J. Neugebauer, J. Phys. Chem. B **112**, 2207 (2008).
[66]J. Neugebauer, J. Chem. Phys. **131**, 084104 (2009).
[67]J. Neugebauer, C. Curutchet, A. Munoz-Losa, and B. Mennucci, J. Chem. Theory Comput. **6**, 1843 (2010).
[68]S. Laricchia, E. Fabiano, and F. Della Sala, J. Chem. Phys. **133**, 164111 (2010).
[69]S. Laricchia, E. Fabiano, and F. Della Sala, Chem. Phys. Lett. **518**, 114 (2011).
[70]C. Huang and E. A. Carter, J. Chem. Phys. **135**, 194104 (2011).
[71]F. Aquilante and T. A. Wesolowski, J. Chem. Phys. **135**, 084120 (2011).
[72]X. Zhou, J. W. Kaminski, and T. A. Wesolowski, Phys. Chem. Chem. Phys. **13**, 10565 (2011).
[73]C. Koenig and J. Neugebauer, Phys. Chem. Chem. Phys. **13**, 10475 (2011).
[74]C. König, N. Schluter, and J. Neugebauer, J. Chem. Phys. **138**, 034104 (2013).
[75]M. Pavanello and J. Neugebauer, J. Chem. Phys. **135**, 234103 (2011).

[76]M. Pavanello, T. Van Voorhis, L. Visscher, and J. Neugebauer, J. Chem. Phys. **138**, 054101 (2013).
[77]M. Pavanello, J. Chem. Phys. **138**, 204118 (2013).
[78]N. Govind, Y. Wang, A. da Silva, and E. Carter, Chem. Phys. Lett. **295**, 129 (1998).
[79]N. Govind, Y. Wang, and E. Carter, J. Chem. Phys. **110**, 7677 (1999).
[80]P. Huang and E. A. Carter, J. Chem. Phys. **125**, 084102 (2006).
[81]D. Lahav and T. Kluener, J. Phys. Condens. Matter **19**, 226001 (2007).
[82]S. Sharifzadeh, P. Huang, and E. A. Carter, Chem. Phys. Lett. **470**, 347 (2009).
[83]S. Höfener and L. Visscher, J. Chem. Phys. **137**, 204120 (2012).
[84]During the reviewing process of this paper, another paper was published [Pavanello *et al.*, J. Chem. Phys. **141**, 174101 (2014)] describing an implementation for periodic subsystem density functional theory similar to the one in the CP2K program (using a pure plane wave code instead of the mixed Gaussian and plane wave approach as employed in CP2K).
[85]J. VandeVondele, U. Borstnik, and J. Hutter, J. Chem. Theory Comput. **8**, 3565 (2012).
[86]K. Kitaura, E. Ikeo, T. Asada, T. Nakano, and M. Uebayasi, Chem. Phys. Lett. **313**, 701 (1999).
[87]R. Z. Khaliullin, E. A. Cobar, R. C. Locha, A. T. Bell, and M. Head-Gordon, J. Chem. Phys. **111**, 8753 (2007).
[88]M. S. Gordon, D. G. Fedorov, S. R. Pruitt, and L. V. Slipchenko, Chem. Rev. **112**, 632 (2012).
[89]H. Reis, M. G. Papadopoulos, and R. W. Munn, J. Chem. Phys. **109**, 6828 (1998).
[90]M. A. Spackman, P. Munshi, and D. Jayatilaka, Chem. Phys. Lett. **443**, 87 (2007).
[91]D. Jayatilaka, P. Munshi, M. J. Turner, J. A. K. Howard, and M. A. Spackman, Phys. Chem. Chem. Phys. **11**, 7209 (2009).
[92]T. Seidler, K. Stadnicka, and B. Champagne, J. Chem. Phys. **139**, 114105 (2013).
[93]G. Lippert, J. Hutter, and M. Parrinello, Mol. Phys. **92**, 477 (1997).
[94]J. VandeVondele, M. Krack, F. Mohamed, M. Parrinello, T. Chassaing, and J. Hutter, Comput. Phys. Commun. **167**, 103 (2005).
[95]A. Seidl, A. Görling, P. Vogl, J. A. Majewski, and M. Levy, Phys. Rev. B **53**, 3764 (1996).
[96]T. Wesolowski and J. Weber, Chem. Phys. Lett. **248**, 71 (1996).
[97]M. V. Berry, Proc. R. Soc. London, Ser. A **392**, 45 (1984).
[98]R. Resta, *Berry Phase in Electronic Wavefunctions*, Troisème Cycle Lecture Notes (Ecole Polytechnique Fédérale, Lausanne, 1996).
[99]R. Resta, Phys. Rev. Lett. **80**, 1800 (1998).
[100]P. L. Silvestrelli, Phys. Rev. B **59**, 9703 (1999).
[101]R. M. Martin and G. Ortiz, Phys. Rev. B **56**, 1124 (1997).
[102]X. Gonze, P. Ghosez, and R. W. Godby, Phys. Rev. Lett. **74**, 4035 (1995).
[103]X. Gonze, P. Ghosez, and R. W. Godby, Phys. Rev. Lett. **78**, 294 (1997).
[104]X. Gonze, P. Ghosez, and R. W. Godby, Phys. Rev. Lett. **78**, 2029 (1997).
[105]P. Ghosez, X. Gonze, and R. W. Godby, Phys. Rev. B **56**, 12811 (1997).
[106]G. Ortiz, I. Souza, and R. M. Martin, Phys. Rev. Lett. **80**, 353 (1998).
[107]R. M. Martin and G. Ortiz, Int. J. Quantum Chem. **69**, 567 (1998).
[108]N. Marzari, A. A. Mostofi, J. R. Yates, I. Souza, and D. Vanderbilt, Rev. Mod. Phys. **84**, 1419 (2012).
[109]T. Wesolowski, J. Am. Chem. Soc. **126**, 11444 (2004).
[110]A. W. Götz, S. Maya Beyhan, and L. Visscher, J. Chem. Theory Comput. **5**, 3161 (2009).
[111]T. A. Wesolowski, Y. Ellinger, and J. Weber, J. Chem. Phys. **108**, 6078 (1998).
[112]T. A. Wesolowski, P.-Y. Morgantini, and J. Weber, J. Chem. Phys. **116**, 6411 (2002).
[113]S. M. Beyhan, A. W. Gotz, and L. Visscher, J. Chem. Phys. **138**, 094113 (2013).
[114]R. Kevorkyants, H. Eshuis, and M. Pavanello, J. Chem. Phys. **141**, 044127 (2014).
[115]S. M. Beyhan, A. W. Götz, C. R. Jacob, and L. Visscher, J. Chem. Phys. **132**, 044114 (2010).
[116]CP2K Developers Group, URL: http://www.cp2k.org.
[117]S. Goedecker, M. Teter, and J. Hutter, Phys. Rev. B **54**, 1703 (1996).
[118]C. Hartwigsen, S. Goedecker, and J. Hutter, Phys. Rev. B **58**, 3641 (1998).
[119]M. Krack, Theor. Chem. Acc. **114**, 145 (2005).
[120]A. D. Becke, Phys. Rev. A **38**, 3098 (1988).
[121]C. Lee, W. Yang, and R. G. Parr, Phys. Rev. B **37**, 785 (1988).
[122]H. Lee, C. Lee, and R. Parr, Phys. Rev. A **44**, 768 (1991).
[123]S. Grimme, J. Antony, S. Ehrlich, and H. Krieg, J. Chem. Phys. **132**, 154104 (2010).
[124]M. Morita, Y. Asai, N. Yoshimoto, and M. Ishikawa, J. Chem. Soc. Faraday Trans. **94**, 3451 (1998).
[125]S. K. Reddy and S. Balasubramanian, J. Phys. Chem. B **116**, 14892 (2012).
[126]S. Nosé, J. Chem. Phys. **81**, 511 (1984).
[127]S. Nosé, Mol. Phys. **52**, 255 (1984).
[128]M. Brehm and B. Kirchner, J. Chem. Inf. Model. **51**, 2007 (2011).
[129]R. Ramírez, T. López-Ciudad, P. Kumar, and D. Marx, J. Chem. Phys. **121**, 3973 (2004).
[130]D. R. Lide, *CRC Handbook of Chemistry and Physics*, 90th ed. (CRC Press, Cleveland, OH, 2009).
[131]S. Luber, M. Iannuzzi, and J. Hutter, J. Chem. Phys. **141**, 094503 (2014).
[132]C. R. Jacob, S. Luber, and M. Reiher, J. Phys. Chem. B **113**, 6558 (2009).
[133]C. R. Jacob, S. Luber, and M. Reiher, Chem.-Eur. J. **15**, 13491 (2009).
[134]S. Luber, J. Phys. Chem. A **117**, 2760 (2013).
[135]J. P. Perdew, Phys. Rev. B **33**, 8822 (1986).
[136]J. P. Perdew, K. Burke, and M. Ernzerhof, Phys. Rev. Lett. **77**, 3865 (1996).
[137]J. P. Perdew, K. Burke, and M. Ernzerhof, Phys. Rev. Lett. **78**, 1396 (1997).
[138]C. Adamo and V. Barone, J. Chem. Phys. **110**, 6158 (1999).
[139]The calculations were performed on one node of a Cray XC30 machine equipped with an 8-core 64-bit Intel SandyBridge CPU (Intel Xeon E5-2670), a NVIDIA Tesla K20X with 6 GB GDDR5 memory and 32 GB of host memory.
[140]M. Guidon, J. Hutter, and J. VandeVondele, J. Chem. Theory Comput. **6**, 2348 (2010).
[141]C. Lee and R. G. Parr, Phys. Rev. A **35**, 2377 (1987).
[142]L. H. Thomas, Proc. R. Soc. London, Ser. A **114**, 561 (1927).
[143]E. Fermi, Rend. Accad. Naz. Lincei **6**, 32 (1927).
[144]J. P. Perdew, Phys. Lett. A **165**, 79 (1992).
[145]F. Tran and T. A. Wesolowski, Int. J. Quantum Chem. **89**, 441 (2002).
[146]A. Lembarki and H. Chermette, Phys. Rev. A **50**, 5328 (1994).
[147]E. W. Pearson and R. G. Gordon, J. Chem. Phys. **82**, 881 (1985).
[148]D. J. Lacks and R. G. Gordon, J. Chem. Phys. **100**, 4446 (1994).
[149]R. Imhof and P. Novák, J. Electrochem. Soc. **145**, 1081 (1998).
[150]D. Aurbach, Y. Gofer, M. Ben-Zion, and P. Aped, J. Electroanal. Chem. **339**, 451 (1992).
[151]K. Xu, Chem. Rev. **104**, 4303 (2004).
[152]P. Verma, P. Maire, and P. Novák, Electrochim. Acta **55**, 6332 (2010).
[153]W. Märkle, C. Y. Lu, and P. Novák, J. Electrochem. Soc. **158**, A1478 (2011).
[154]S. Pérez-Villar, P. Lanz, H. Schneider, and P. Novák, Electrochim. Acta **106**, 506 (2013).
[155]K. Hongyou, T. Hattori, Y. Nagai, T. Tanaka, H. Nii, and K. Shoda, J. Power Sources **243**, 72 (2013).
[156]K. Leung, J. Phys. Chem. C **117**, 1539 (2013).
[157]K. Leung, Chem. Phys. Lett. **568–569**, 1 (2013).
[158]R. Jorn, R. Kumar, D. P. Abraham, and G. A. Voth, J. Phys. Chem. C **117**, 3747 (2013).
[159]D. Aurbach, Y. Ein-Eli, O. Chusid, Y. Carmeli, M. Babai, and H. Yamin, J. Electrochem. Soc. **141**, 603 (1994).
[160]F. Joho and P. Novák, Electrochim. Acta **45**, 3589 (2000).
[161]M. D. Bhatt, M. Cho, and K. Cho, Modell. Simul. Mater. Sci. Eng. **20**, 065004 (2012).
[162]J. L. Alonso, R. Cervellati, A. Esposti, D. Lister, and P. Palmier, J. Chem. Soc., Faraday Trans. 2 **82**, 357 (1986).
[163]R. S. Mulliken, J. Chem. Phys. **23**, 1833 (1955).
[164]J. Nafziger and A. Wasserman, J. Phys. Chem. A **118**, 7623 (2014).